

# Electrospun Polyimide Nanocomposite Fibers Reinforced with Core-Shell Fe-FeO Nanoparticles

Jiahua Zhu,<sup>†</sup> Suying Wei,<sup>‡</sup> Xuelong Chen,<sup>†</sup> Amar B. Karki,<sup>§</sup> Dan Rutman,<sup>†</sup> David P. Young,<sup>§</sup> and Zhanhu Guo<sup>\*,†</sup>

*Integrated Composites Laboratory (ICL), Dan F. Smith Department of Chemical Engineering, Lamar University, Beaumont, Texas 77710, Department of Chemistry and Physics, Lamar University, Beaumont, Texas 77710, and Department of Physics and Astronomy, Louisiana State University, Baton Rouge, Louisiana 70803*

*Received: March 5, 2010; Revised Manuscript Received: April 14, 2010*

Both pure polyimide (PI) and Fe-FeO nanoparticles reinforced PI nanocomposite fibers with a particle loading of 5, 10, 20, and 30 wt % are produced by electrospinning with optimized operational parameters such as polymer concentration, applied electrical voltage, and tip-to-collector distance. The morphology of the resulting products is correlated to the corresponding rheological behaviors of the pure PI and Fe-FeO/PI nanocomposite solutions. Thermogravimetric analysis (TGA) and differential scanning calorimetry (DSC) reveal an enhanced thermal stability of the nanocomposite fibers after introducing the Fe-FeO nanoparticles. The glass transition temperature ( $T_g$ ) and melting temperature ( $T_m$ ) of the nanocomposite fibers increase by 10–12 and 15–17 °C, respectively, as compared to those of the pure PI fibers. The magnetic properties of the Fe-FeO nanoparticles in the polymer nanocomposite fibers are different from those of the as-received nanoparticles. An increased shell thickness by 7.4% is deduced after the nanoparticles experiencing the high-voltage electrospinning.

## 1. Introduction

Polymer nanocomposites (PNCs) or organic-inorganic hybrids attain the advantages of the polymers such as light weight, easy processability, and flexibility, and introduce the propensity of the inorganic materials such as high mechanical strength and excellent electrical, magnetic, and optical properties. Sometimes, PNCs even possess unique physical, chemical, or biological properties, which are essentially different from those of the components taken separately or physically combined properties of each component. These PNCs have attracted wide interest in both academic and industrial fields for their diverse potential applications in energy storage devices,<sup>1</sup> electronics,<sup>2,3</sup> microwave absorbers,<sup>4,5</sup> and sensors.<sup>6</sup>

Electrospinning technology has attracted much interest recently owing to its comparatively low manufacturing cost and high production for fabricating polymeric micro- and nanofibers in large scale as compared to other technologies, such as melt fibrillation,<sup>7</sup> nanolithography,<sup>8</sup> and self-assembly.<sup>9,10</sup> Electrospun fibers, especially in the nanoscale size, have found wide applications in various fields. For example, electrospun nanofibers possessing high porosity and large surface-to-volume ratio have been used as membranes for gas separation, protein purification, and wastewater treatment.<sup>11–13</sup> However, polymer fibers have major disadvantages such as inferior thermal stability,<sup>14</sup> low mechanical strength, and solvent absorption (swelling effect) when exposed to liquid or gas.<sup>15</sup> Various nanomaterials have been introduced to the polymer matrix with an aim to enhance the physical, chemical, and biological properties of the polymer fibers. Meanwhile, the specific unique properties of the nanomaterials would be combined with the

nanocomposite fibers. Composite nanofibers with enhanced mechanical and thermal properties have been reported in polymer blends and inorganic-organic composites.<sup>16,17</sup> Wang et al.<sup>18</sup> electrospun poly(vinyl acetate)/tungsten isopropoxide (PVAc/W(<sup>i</sup>Pr)<sub>6</sub>) nanocomposite fibers, which are transformed to polycrystalline WO<sub>3</sub> nanofibers for ammonia gas detection.

Polyimides (PIs), a class of high-performance engineering plastics, are well-known for their excellent mechanical properties, stability at high temperatures, superior dielectric properties, and good chemical resistance. PI has been applied in aerospace, automobile, and microelectronic industries.<sup>19,20</sup> PI has been used as a carbon precursor to fabricate magnetic carbon composite films.<sup>21,22</sup> Clay<sup>23</sup> and montmorillonite<sup>24,25</sup> (MMT) functionalized with organics have been studied for their significant contribution to the enhanced thermal and mechanical properties of PI nanocomposites. The dielectric constant of polyhedral oligomeric silsesquioxan (POSS)/PI nanocomposites was reduced by 9.1% with the incorporation of 2.5 mol % POSS while maintaining the mechanical properties.<sup>26</sup> Various other nanoparticles, such as zirconium tungstate (ZrW<sub>2</sub>O<sub>8</sub>),<sup>27</sup> aluminum nitride (AlN),<sup>28</sup> BaTiO<sub>3</sub>,<sup>29</sup> and TiO<sub>2</sub><sup>30</sup> were also introduced in PI matrix to obtain versatile unique properties. Siochi et al.<sup>31</sup> produced single-walled carbon nanotubes/PI nanocomposite fibers with improved tensile moduli and yield stress using a melt processing method. However, the fabrication of PI nanocomposites with the electrospinning method is rarely reported, even less for the polyimide nanocomposites filled with magnetic nanoparticles.

Fe-Fe core-shell (Fe@FeO) structured nanoparticles are chosen due to their relatively high stability in air over that of the pure iron nanoparticles while maintaining superior magnetic properties. The thermal stability and magnetic properties of the PI nanocomposite fibers are expected for high-temperature magnetic sensing and microwave absorption applications.

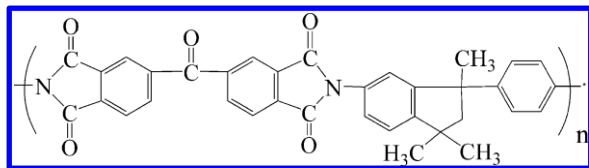
In this work, pure PI and Fe-FeO/PI nanocomposite fibers with various Fe@FeO nanoparticle loadings (5, 10, 20, and 30

\* To whom correspondence should be addressed. E-mail: zhanhu.guo@lamar.edu. Phone: (409) 880-7654. Fax: (409) 880-7283.

<sup>†</sup> Integrated Composites Laboratory (ICL), Dan F Smith Department of Chemical Engineering, Lamar University.

<sup>‡</sup> Department of Chemistry and Physics, Lamar University.

<sup>§</sup> Department of Physics and Astronomy, Louisiana State University.

**SCHEME 1: Molecular Structure of Polyimide (Matrimid 5218 US)**


wt %) are fabricated by the electrospinning process. Both electrospinning and electrospinning phenomena are observed in polymer solutions with different polymer concentrations. The effects of polymer concentration, applied electrical voltage, and tip-to-collector distance on the fiber morphology and size distribution are systematically studied. Thermal stability and magnetic properties of the nanocomposite fibers are investigated in this work. The core-shell structure of the nanoparticles is deduced to change after the high-voltage electrospinning.

## 2. Experimental Section

**2.1. Materials.** Polyimide (PI, powder, Matrimid 5218 US) was supplied by Huntsman Advanced Materials Americas, Inc. Scheme 1 shows the molecular structure of PI. Core-shell Fe-FeO nanoparticles with an average size of 20 nm are provided by QuantumSphere, Inc. *N,N*-Dimethylformamide (DMF, 99.9%, anhydrous) was purchased from Fisher Scientific Inc. All the materials were used as received without any further treatment.

**2.2. Preparation of Polyimide and Nanocomposite Solutions.** The PI/DMF solutions with PI loading of 10 and 20 wt % are prepared by magnetic stirring overnight to completely dissolve the polymer at room temperature. Nanocomposite solutions are prepared from 20 wt % PI/DMF solution. Fe-FeO nanoparticles (5, 10, 20, and 30 wt %, with regard to the weight of PI) are weighed in different beakers, and then the specific amount of 20 wt % PI/DMF solution is added. After completely wetting the nanoparticles with the polymer solution, both mechanical stirring (600 rpm, 1 h) and ultrasonication (40 min) are subsequently performed to disperse the nanoparticles in PI/DMF solution. Both pure polymer and Fe-FeO/PI nanocomposite solutions are used for electrospinning. All the experiments are performed at room temperature.

**2.3. Fabrication of Pristine PI and Nanocomposite Fibers.** Pure PI and Fe-FeO/PI nanocomposite fibers are prepared by electrospinning. The viscous polymer solutions are loaded in a 10 mL syringe equipped with a 0.80 mm (inner diameter) stainless steel gauge needle. The needle is connected to a high-voltage power supply (Gamma High Voltage Research, Product HV power supply, Model No. ES3UP-5w/DAM), which is capable of providing a DC voltage up to 30 kV. The grounded counter electrode is a flat aluminum foil. The solution is constantly and continuously supplied with use of a syringe pump (NE-300, New Era Pump System, Inc.). Various feedrates are studied from 0.05 to 0.5  $\mu\text{L}/\text{min}$  and the optimal feedrate is chosen at 0.1  $\mu\text{L}/\text{min}$  based on the experimental observations. The applied voltage in this work is adjusted from 10 to 25 kV. The external electrical field applied to the polymer solution through the positive electrode is able to overcome the surface tension of the various solutions and form a polymer jet, which forms fibers on the aluminum foil after solvent evaporation. The fibers are dried at 80  $^{\circ}\text{C}$  in a vacuum oven and stored for further characterization.

**2.4. Characterization.** The rheological behavior of the pure PI and its nanocomposite solutions are investigated with an AR 2000ex Rheometer (TA Instrumental Company) at a shear rate

ranging from 1 to 100 1/s at 25  $^{\circ}\text{C}$ . A series of measurements are performed in a cone-and-plate geometry with a diameter of 40 mm and a truncation of 66  $\mu\text{m}$ .

Fourier transform infrared spectroscopy (FT-IR, Bruker Inc. Vector 22 FT-IR spectrometer, coupled with an ATR accessory) is used to characterize the pure PI and its nanocomposite fibers in the range of 500 to 4000  $\text{cm}^{-1}$  at a resolution of 4  $\text{cm}^{-1}$ .

The glass transition temperature ( $T_g$ ) and melting temperature ( $T_m$ ) are investigated by differential scanning calorimetry (DSC 2010, TA Instruments) with a heating rate of 10  $^{\circ}\text{C}/\text{min}$  and a nitrogen flow rate of 20 mL/min. The samples are sealed in a Tzero Pan (TA Instruments) and the measurement is conducted in the temperature range of 25–300  $^{\circ}\text{C}$ . The weight of each sample is about 10 mg. The DSC heat flow and temperature are calibrated with an indium standard.

The thermal stability of PI and its nanocomposite fibers with different nanoparticle loadings is studied with a thermogravimetric analysis (TGA, TA Instruments TGA Q-500). TGA is conducted on the pure PI and its Fe-FeO nanocomposite fibers from 25 to 900  $^{\circ}\text{C}$  with a nitrogen flow rate of 60 mL/min and a heating rate of 10 deg/min.

The morphology of the pure PI and Fe-FeO/PI nanocomposite fibers is evaluated by scanning electron microscopy (Hitachi S-3400 scanning electron microscopy).

The magnetic properties of the Fe-FeO nanoparticles and Fe-FeO/PI nanocomposite fibers at room temperature are carried out in a 9 T physical properties measurement system (PPMS) by Quantum Design.

## 3. Results and Discussion

**3.1. Microstructure of Pure Polyimide Fibers. 3.1.1. Polymer Concentration Effect.** Electrospinning and electrospinning are two different processes for fabricating micrometer and submicrometer sized materials from polymers either in solutions or melts.<sup>32–34</sup> The process can be controlled from one to the other by adjusting the operational parameters, though many operational parameters may affect the size and morphology of the final products, such as polymer concentration (viscosity),<sup>35,36</sup> spinning atmosphere,<sup>37</sup> applied electrical voltage, and tip-to-target distance.<sup>38</sup> The surface tension of the solution and the electrostatic force should be balanced to obtain the stable jets in order for fiber formation. Once the applied voltage exceeds the critical voltage, the stable jets of liquids will be ejected from the cone tip. The jets will break up into droplets and form particles if the solution viscosity is extremely low, such as the 10 wt % PI/DMF solution, which only shows an average viscosity of 0.09 Pa·s within the shear rate range from 1 to 100 1/s, Figure 1a. The viscosity sharply increases to 3.15 Pa·s when the polymer concentration increases to 20 wt %. Moreover, a corresponding higher viscosity is observed with the increase of the nanoparticle loading. Figure 1b shows the corresponding shear stress (Pa) as a function of shear rate (1/s) for the polymer solutions with different particle loadings. The shear stress is observed to increase almost linearly with the increase of the shear rate, indicating a Newtonian fluid behavior. The low viscous solution (10 wt % PI/DMF) is observed to form droplets under the electrical field, Figure 2a,b. Microparticles with diameters varying from submicrometer to micrometer are observed and the submicrometer spheres are connected by nanosized fibers. The formed submicrometer spheres with a narrow size distribution rather than the continuous polymer fibers are arising from the electrospinning modes.<sup>39,40</sup> For the polymer solutions with high viscosity, 20 wt % PI/DMF solution (3.15 Pa·s, Figure 1a) in this case, the jet without breaking up

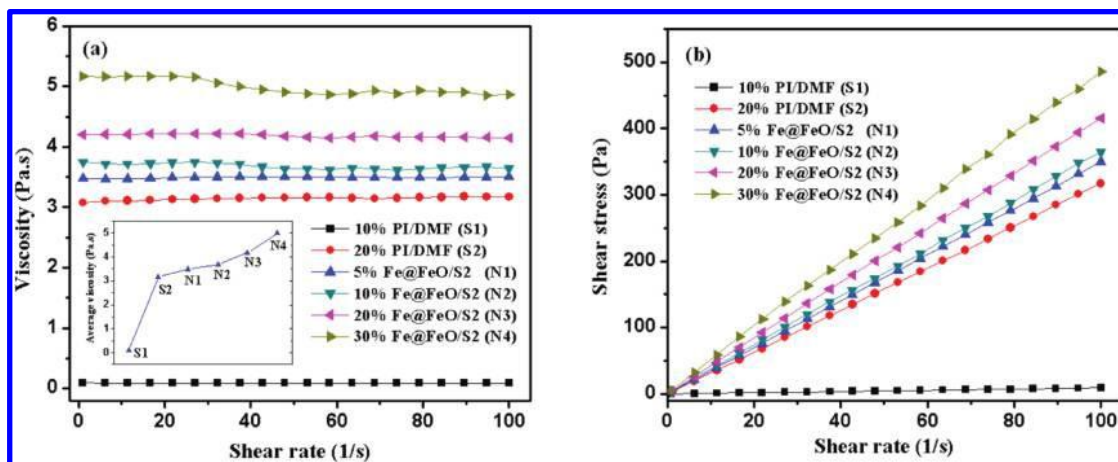


**Figure 1.** (a) Viscosity of 10 wt % PI/DMF (S1), 20 wt % PI/DMF (S2) and nanocomposite solutions with Fe@FeO nanoparticle loadings of 5 (N1), 10 (N2), 20 (N3), and 30 wt % (N4), respectively. The inset figure is the average viscosity calculated from the whole shear range. (b) Shear stress vs shear rate of the solutions.

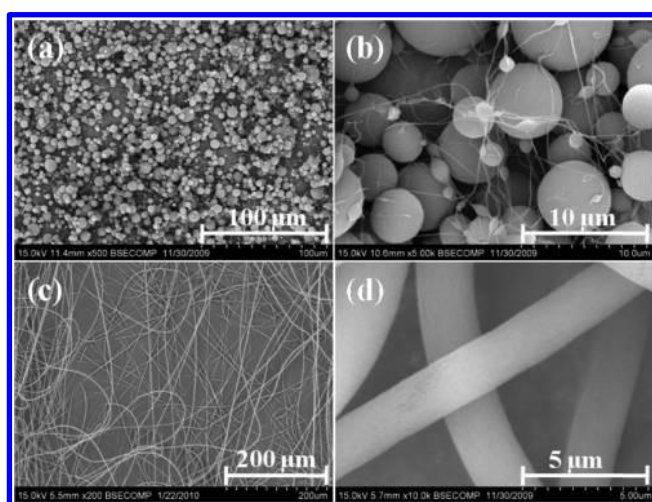


**Figure 2.** SEM microstructures of (a, b) 10 wt % PI/DMF solution and (c, d) 20 wt % PI/DMF solution (15 cm and 15 kV).

due to the cohesive nature of the high viscosity, travels to and finally forms the fibers on the collecting grounded electrode, Figure 2c,d. The formed fibers are uniform without any beads. High magnification observation does not show any pore on the surface of the particles, Figure 2b, and of the fibers, Figure 2d.

**3.1.2. Tip-to-Collector Distance and Applied Voltage Effects.** The effects of the tip-to-collector distance and the applied electrical voltage on the fiber morphology and size distribution are investigated. The experiments are set at different distances (15 and 20 cm) and various voltages (10, 12, and 15 kV) while maintaining a constant 20 wt % PI/DMF solution. Figure 3 shows the fiber morphology and specific fiber size. Panels a and d of Figure 3 show the microstructures of the fibers prepared with an applied constant electrical voltage of 10 kV and a working distance of 15 and 20 cm, respectively. The fiber exhibits larger diameter size from 10 to 20 μm with a shorter tip-to-collector distance, Figure 3a. However, the fibers are observed nonuniformly distributed and the sizes can be generally divided into two groups: one is the larger fibers with a size of about 10 μm and the other is in the size of 1 μm. This observation is consistent with the results obtained in poly(ethylene oxide) (PEO)/water solution, which shows an obvious more secondary population of fibers with diameters about one-third of those in the primary population.<sup>32</sup> In our case, the secondary fiber diameter is much smaller, which is only about 1/10 of the primary fiber diameter. The secondary population of fibers observed

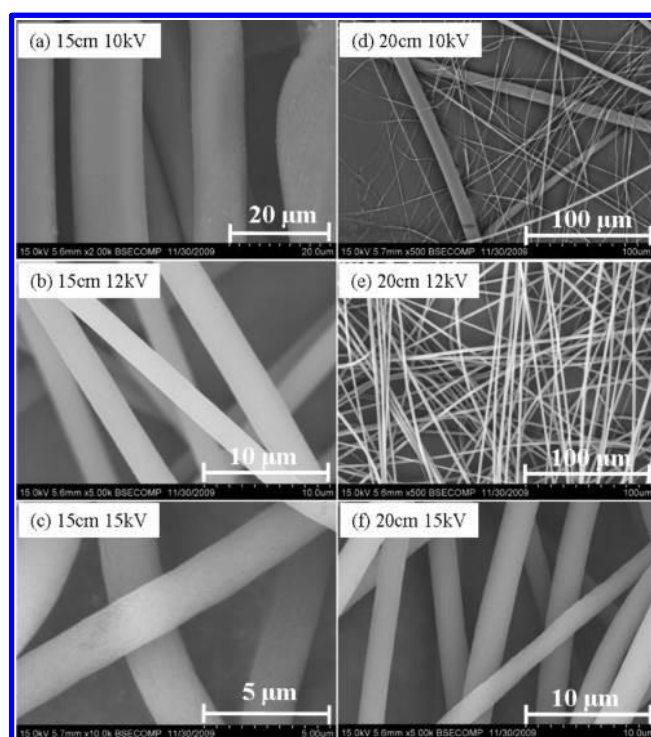


**Figure 3.** SEM images of the pure PI fibers obtained at different operational conditions (20 wt % PI/DMF solution).

in the electrospun fibers is formed due to the fiber splaying, which is also observed in other works.<sup>41</sup>

The fibers exhibit uniform size distribution when the applied electrical voltage increases to 12 and 15 kV. High voltage is able to generate more charges to the solution or droplet surface located at the tip of the needle (larger columbic forces) as well as stronger electrical field (larger electrostatic forces), both of which stretch the jets fully for the favorable formation of the uniform and smooth fibers.<sup>42,43</sup> However, the tip-to-collector distance seems to have no significant effect on the fiber morphology and size distribution, the diameter is about 2–4 μm for the fibers fabricated under different conditions, Figure 3, panels b and c, and e and f. These results indicate that the accelerating voltage is the prominent factor to obtain uniform fibers when polymer solutions with high concentrations are used.

**3.2. Microstructure of Fe-FeO/PI Nanocomposite Fibers.** Fe-FeO/PI nanocomposite fibers are fabricated with different Fe-FeO nanoparticle loadings from 5 to 30 wt %. Figure 4 shows

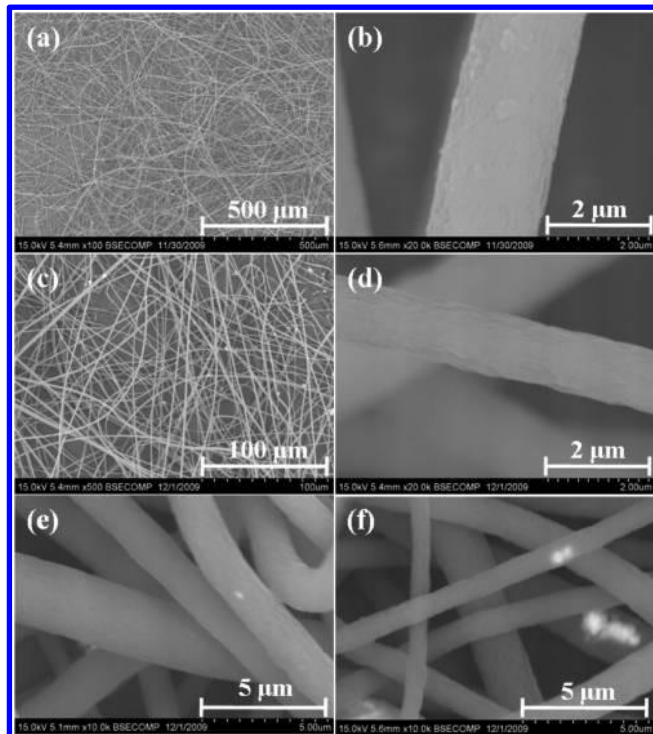


**Figure 4.** SEM images of Fe@FeO/PI nanocomposite fibers with different nanoparticle loadings: (a, b) 5 wt % Fe@FeO/PI, 15 cm, 12 kV; (c, d) 10 wt % Fe@FeO/PI, 15 cm, 17 kV; (e) 20 wt % Fe@FeO/PI, 20 cm, 22 kV; and (f) 30 wt % Fe@FeO/PI, 20 cm, 25 kV.

the SEM microstructures of the nanocomposite fibers with different particle loadings. The solutions with higher nanoparticle loadings are observed to require larger applied electrical voltages to obtain nanocomposite fibers due to the increased viscosity as particle loadings increase, Figure 1a. The viscosity increases gradually from 3.15 to 4.99 Pa · s as the particle loading increases from 5 to 30 wt %. To be specific, high electrical voltage provides larger electrical force between the tip of the needle and the collecting electrode, which is used to overcome the enhanced internal adhesion force and larger surface tension of the polymer solutions introduced by the addition of nanoparticles. The fibers are observed almost constant at around 2  $\mu\text{m}$  for each composition and the nanoparticles are well dispersed in the polymer fiber matrix, Figure 4. However, Figure 4f shows slight agglomeration of nanoparticles as the particle loading increases to 30 wt %. The surface of nanocomposite fibers is relatively rougher as compared to that of the pure PI fibers. The more viscous nanocomposite solutions retard the solvent evaporation process, which introduces more relaxation time for polymer chains. And the introduced nanoparticles restrict the motion of the polymer chain. Under such circumstances, the polymer chains are less patterned as compared to the pure PI fibers, thus show a rougher surface.

**3.3. FT-IR Analysis.** Figure 5 shows the FT-IR spectra of the pure PI and Fe-FeO/PI nanocomposite fibers. The bands at 859, 831, and 715  $\text{cm}^{-1}$  are assigned to the 1,2,4-trisubstitute of the benzene structure and the bands at 1508 and 1486  $\text{cm}^{-1}$  are attributed to the backbone vibration of C-C in the benzene ring. The strong band at 1370  $\text{cm}^{-1}$  indicates the C-N stretching in the polymer backbone structure.<sup>44</sup> The asymmetric and symmetric stretching bands of the -CO- are shown at 1668 and 1720  $\text{cm}^{-1}$ , respectively.<sup>45</sup> The presence of the bands in the region of 1000-1250  $\text{cm}^{-1}$  is attributed to the vibration and stretching of various methyl groups (-CH<sub>3</sub>, -C(CH<sub>3</sub>)<sub>2</sub>). All these characteristic bands in the FT-IR spectra confirm the

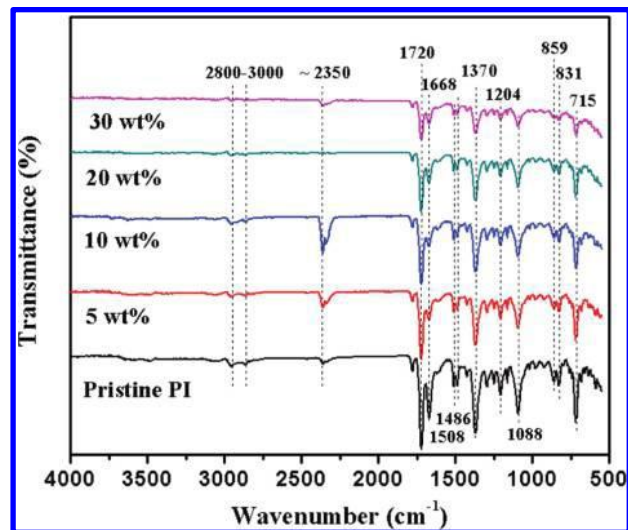


**Figure 5.** FT-IR spectra of pristine PI fibers and Fe@FeO/PI nanocomposite fibers with different particle loadings.

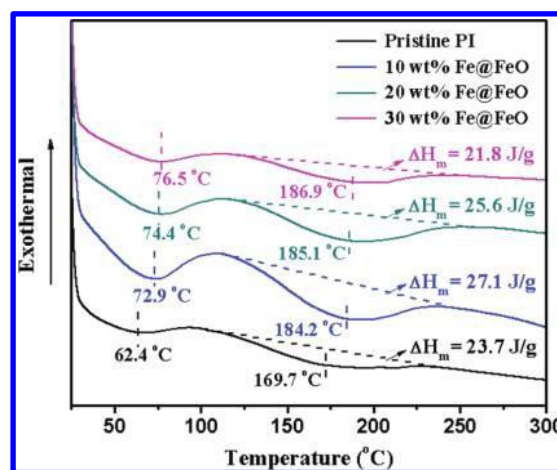


**Figure 6.** DSC thermograms of pristine PI fibers and nanocomposite fibers with different nanoparticle loadings.

molecular structure of the PI, Figure 5. Also, the molecular structure is well maintained after dissolving in DMF and being fabricated into fibers at the high electric field. As compared to the spectrum of the pure PI fibers, no additional bands are observed in the spectra of its nanocomposite fibers. This indicates that the nanoparticles and PI matrix are physically entangled together rather than through the formed chemical bonding to form the nanocomposites.

**3.4. DSC Analysis.** Figure 6 shows the DSC curves of pure PI and Fe-FeO/PI nanocomposite fibers. Two endothermic dips are observed from the curves. The first dip at around 70  $^{\circ}\text{C}$  indicates the glass transition temperature ( $T_g$ ) and the second dip at around 180  $^{\circ}\text{C}$  represents the melting temperature ( $T_m$ ), respectively. It is evident that both  $T_g$  and  $T_m$  increase with the increase of the nanoparticle loading. The  $T_g$  for the pure PI fibers is 62.4  $^{\circ}\text{C}$  and increases to 72.9, 74.4, and 76.5  $^{\circ}\text{C}$  for the nanocomposite fibers with a particle loading of 10, 20, and 30 wt %, respectively. A similar phenomenon has been observed in organically modified layered silicates/epoxy nanocomposites, where the DSC results show a continuous increase in  $T_g$  with the addition of the layered silicates.<sup>46</sup> The increase in  $T_g$  observed in the PI nanocomposites with all nanoparticle loadings is attributed to the interactions between the nanoparticles and PI matrix<sup>46,47</sup> and the nanoconfinement of nanoparticles on the polymer chains, which restrict the segmental motions at the organic-inorganic interface.<sup>48</sup>

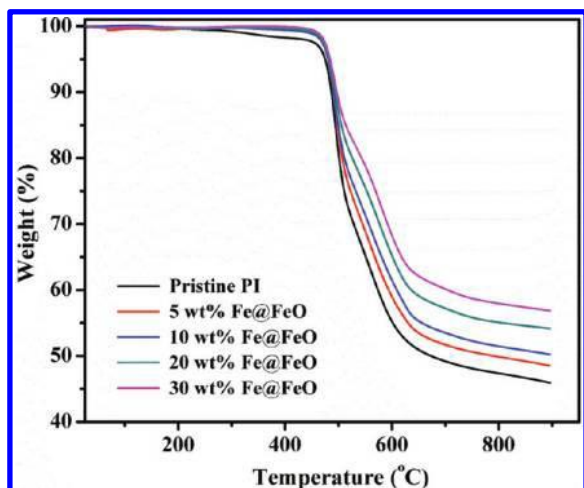


**Figure 7.** Thermogravimetric curves for the pristine PI and nanocomposite fibers.

**TABLE 1: TGA Results of PI and Fe@FeO/PI Nanocomposite Fibers**

samples	$T_{5\%}$ (°C)	wt residue at 400 °C (%)
pristine PI	473.8	98.3
5 wt % Fe@FeO/PI	480.6	99.8
10 wt % Fe@FeO/PI	481.9	99.7
20 wt % Fe@FeO/PI	482.9	99.6
30 wt % Fe@FeO/PI	484.3	99.9

A similar trend in  $T_m$  is also observed for the pure PI fibers and Fe@FeO/PI nanocomposite fibers, Figure 6. The  $T_m$  is enhanced by 14.5 °C for the nanocomposite fibers with a 10 wt % particle loading and is slightly increased by 1-2 °C with the particle loading further increases to 20 and 30 wt %. The increased melting temperature is due to the retarded mobility of the PI chains induced by Fe@FeO nanoparticles and subsequently higher energy is needed to move the whole long polymer chains.

The melting enthalpy ( $\Delta H_m$ , based on the weight of pure polymer rather than the total weight of polymer nanocomposites) is observed to increase from 23.7 J/g for pure polyimide to 27.1 J/g for the Fe@FeO/PI nanocomposite fibers with a 10 wt % particle loading, which is due to the reduced mobility of the polymer chains induced by the nanoparticles. However, the  $\Delta H_m$  decreases gradually to 25.6 and 21.8 J/g when the nanoparticle loading further increases to 20 and 30 wt %, respectively. Similar results were also observed in iron oxide/PVA nanocomposites at higher particle loadings.<sup>49</sup>

**3.5. Thermogravimetric Analysis (TGA).** Figure 7 shows the thermal gravimetric curves of the pure PI and Fe@FeO/PI nanocomposite fibers up to 900 °C. The initial thermal decomposition temperatures ( $T_{5\%}$ , the temperature at which the total mass loss of 5% occurs) of all the samples are obtained and summarized in Table 1.  $T_{5\%}$  is observed to increase significantly with the increase of the Fe@FeO nanoparticle loadings due to the restriction of the nanoparticles on the long-range chain mobility of the polyimide phase within the nanocomposites. Similar results are also reported in the poly(vinyl chloride) (PVC)/CaCO<sub>3</sub> nanocomposites<sup>50</sup> and poly(vinyl acetate) (PVAc)/silicate nanocomposites.<sup>51</sup> In addition, the thermal stability of PI in the temperature range of 300-400 °C demonstrates the capability to process these nanocomposites within this temperature range, Table 1. The less weight loss of the Fe@FeO/PI nanocomposite fibers at 400 °C is much lower than that of the pristine PI fibers, which indicates an improved thermal stability and is beneficial to the industrial manufacturing.

**3.6. Magnetic Property.** Figure 8 shows the room temperature magnetic hysteresis loops of the as-received Fe@FeO nanoparticles and Fe@FeO/PI nanocomposite fibers with a nanoparticle loading of 30 wt %. The saturation magnetization ( $M_s$ ) is defined at the state when an increase in the magnetic field cannot increase the magnetization of the material further.  $M_s$  of both the as-received Fe@FeO nanoparticles and Fe@FeO/PI nanocomposite fibers are observed to be reached at a relatively high magnetic field.  $M_s$  is 108.1 and 30.6 emu/g for the as-received Fe@FeO nanoparticles and its nanocomposite

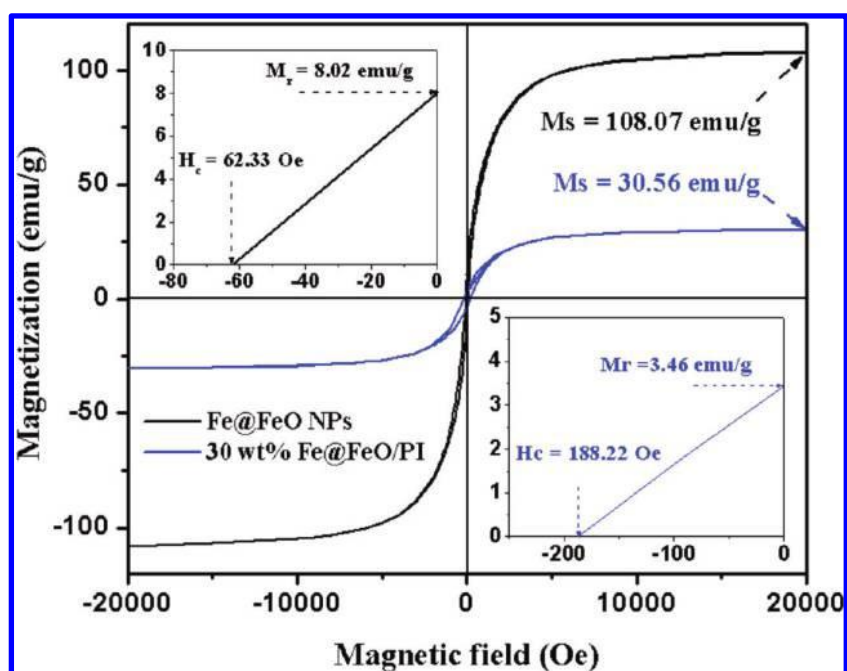


**Figure 8.** Hysteresis loops of the as-received Fe@FeO nanoparticles and Fe@FeO/PI nanocomposite fibers with 30 wt % particle loading at room temperature.

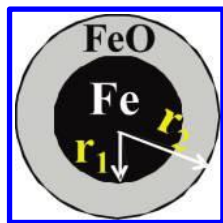


**Figure 9.** The schematic graph of the core-shell structured Fe@FeO nanoparticle.

fibers with a loading of 30%, respectively. The coercivity ( $H_c$ , Oe) indicates the external applied magnetic field necessary to return the material to a zero magnetization condition, and the remnant magnetization ( $M_r$ ) is the residue magnetization after the applied field is reduced to zero. Both values can be read from the axes crossing points, Figure 8 (inset figures). The coercivity increases from 62.3 Oe for Fe@FeO nanoparticles to 188.2 Oe after the nanoparticles are dispersed in the PI matrix. This indicates that the Fe@FeO nanoparticles become magnetically harder after being dispersed in the PI matrix within the nanocomposite fibers. The enhanced coercivity of nanoparticles is due to the decreased interparticle dipolar interaction, which arises from the enlarged nanoparticle spacer distance for the single domain nanoparticles,<sup>38,52,53</sup> as compared to the closer contact of the pure nanoparticles.

In this work, the shell thickness of the nanoparticles before and after electrospinning is calculated according to the following equation:

$$\frac{4}{3}\pi r_1^3 \rho_{\text{Fe}} M_{\text{s(Fe)}} + \frac{4}{3}\pi (r_2^3 - r_1^3) \rho_{\text{FeO}} M_{\text{s(FeO)}} = M_{\text{s(Fe@FeO)}} \quad (1)$$

where  $r_1$  and  $r_2$  represent the radius of core (Fe) and Fe@FeO nanoparticle, respectively. The schematic structure of the nanoparticle is depicted in Figure 9.  $M_{\text{s(Fe)}}$  and  $M_{\text{s(FeO)}}$  are saturated magnetization of bulk Fe and FeO with a reported value of 218 emu/g for Fe<sup>54</sup> and 47.4 emu/g for FeO.<sup>55</sup>  $\rho_{\text{Fe}}$  and  $\rho_{\text{FeO}}$  are the densities of pure bulk iron and iron(II) oxide ( $\rho_{\text{Fe}}$  7.87 g/cm<sup>3</sup>;  $\rho_{\text{FeO}}$  5.70 g/cm<sup>3</sup>).  $M_{\text{s(Fe@FeO)}}$  is the measured saturated magnetization value of the pure Fe@FeO nanoparticles. Taking the average diameter of the nanoparticle as 20 nm, the radius of the core ( $r_1$ ) and shell ( $r_2 - r_1$ ) is calculated to be 13.2 and 6.8 nm, respectively. Theoretically,  $M_s$  for the Fe@FeO/PI nanocomposite fibers with a particle loading of 30 wt % is 32.4 emu/g. However, the measured value is 30.6 emu/g, which is slightly lower than the theoretical value. On the basis of the measured  $M_s$  of the nanocomposites, the calculated  $r_1$  and  $r_2$  are 12.7 and 7.3 nm, respectively. This indicates a reduced core and an increased shell thickness, which is arising from the further particle oxidation at extremely high voltages during the electrospinning process.

#### 4. Conclusion

Pure PI and Fe@FeO/PI nanocomposites fibers are produced by electrospinning. The effects of polymer concentration, acceleration voltage, and tip-to-collector distance on the morphology and size distribution of the fibers are systematically studied. Higher voltage is required for the fabrication of nanocomposite fibers at high nanoparticle loadings owing to the increased viscosity of the nanocomposite solutions. TGA and DSC results indicate an enhanced thermal stability with an increased glass transition ( $T_g$ ) temperature of the nanocomposite fibers as compared to that of the pure PI fibers. The nanoparticles

in the nanocomposites fibers become magnetically harder with a significant increase of coercivity from 62.3 Oe (as-received Fe@FeO nanoparticles) to 188.2 Oe. Meanwhile, an increase of about 7.4% in the nanoparticle shell thickness is deduced during the high-voltage electrospinning fiber fabrication process.

**Acknowledgment.** This work is supported by the research start-up fund and research enhancement grant from Lamar University. D.P.Y. acknowledges support from the NSF under Grant No. DMR 04-49022. The financial support from the Dan F. Smith Department of Chemical Engineering and College of Engineering at Lamar University for obtaining the TA rheometer is kindly acknowledged.

#### References and Notes

- (1) Kim, P.; Doss, N. M.; Tillotson, J. P.; Hotchkiss, P. J.; Pan, M.-J.; Marder, S. R.; Li, J.; Calame, J. P.; Perry, J. W. *ACS Nano* **2009**, *3*, 2581–2592.
- (2) Vacca, P.; Nenna, G.; Miscioscia, R.; Palumbo, D.; Minarini, C.; Sala, D. D. *J. Phys. Chem. C* **2009**, *113* (14), 5777–5783.
- (3) Nogueira, A. F.; Lomba, B. S.; Soto-Oviedo, M. A.; Correia, C. R. D.; Corio, P.; Furtado, C. A.; Hummelgen, I. A. *J. Phys. Chem. C* **2007**, *111*, 18431–18438.
- (4) Guo, Z.; Park, S.; Hahn, H. T.; Wei, S.; Moldovan, M.; Karki, A. B.; Young, D. P. *J. Appl. Phys.* **2007**, *101*, 09M511.
- (5) Guo, Z.; Lee, S. E.; Kim, H.; Park, S.; Hahn, H. T.; Karki, A. B.; Young, D. P. *Acta Mater.* **2009**, *57*, 267–277.
- (6) Shimada, T.; Ookubo, K.; Komuro, N.; Shimizu, T.; Uehara, N. *Langmuir* **2007**, *23*, 11225–11232.
- (7) Perez, M. A.; Swan, M. D.; Louks, J. W. US Pat. 6, 110, 588, 2000.
- (8) Daan, W.; Ulrich, S. S. *Angew. Chem., Int. Ed.* **2004**, *43*, 2480–2495.
- (9) Faul, C. F. J.; Antonietti, M. *Adv. Mater.* **2003**, *15*, 673–683.
- (10) Whitesides, G. M.; Boncheva, M. *Proc. Natl. Acad. Sci. U.S.A.* **2002**, *99*, 4769–4774.
- (11) Wang, D.; Li, K.; Teo, W. K. *J. Membr. Sci.* **1996**, *115*, 85–108.
- (12) Ma, Z.; Kotaki, M.; Ramakrishna, S. *J. Membr. Sci.* **2006**, *272*, 179–187.
- (13) Shimizu, Y.; Okuno, Y.-I.; Uryu, K.; Ohtsubo, S.; Watanabe, A. *Water Res.* **1996**, *30*, 2385–2392.
- (14) Krzysztosf, P.; Njuguna, J. *Thermal degradation of polymeric materials*; Rapra Technology: Shawbury, UK, 2005.
- (15) Wind, J. D.; Sirard, S. M.; Paul, D. R.; Green, P. F.; Johnston, K. P.; Koros, W. J. *Macromolecules* **2003**, *36*, 6442–6448.
- (16) Liu, R.; Cai, N.; Yang, W.; Chen, W.; Liu, H. *J. Appl. Polym. Sci.* **2009**, *116*, 1313–1321.
- (17) Naebe, M.; Lin, T.; Staiger, M. P.; Dai, L.; Wang, X. *Nanotechnology* **2008**, *19*, 305702/1–8.
- (18) Wang, G.; Ji, Y.; Huang, X.; Yang, X.; Gouma, P.-I.; Dudley, M. *J. Phys. Chem. B* **2006**, *110*, 23777–23782.
- (19) Weiser, E. S.; Johnson, T. F.; St Clair, T. L.; Echigo, Y.; Kaneshiro, H.; Grimsley, B. W. *High Perform. Polym.* **2000**, *12*, 1–12.
- (20) Bradley, K.; Gabriel, J.-C. P.; Gruner, G. *Nano Lett.* **2003**, *3*, 1353–1355.
- (21) Inagaki, M.; Oka, H.; Kaburagi, Y.; Hishiyama, Y. *Solid State Ionics* **1999**, *121*, 157–163.
- (22) Kaburagi, Y.; Hishiyama, Y.; Oka, H.; Inagaki, M. *Carbon* **2001**, *39*, 593–603.
- (23) Tyan, H.-L.; Liu, Y.-C.; Wei, K.-H. *Chem. Mater.* **1999**, *11*, 1942–1947.
- (24) Magaraphan, R.; Lilayuthalart, W.; Sirivat, A.; Schwank, J. W. *Compos. Sci. Technol.* **2001**, *61*, 1253–1264.
- (25) Tyan, H.-L.; Leu, C.-M.; Wei, K.-H. *Chem. Mater.* **2000**, *13*, 222–226.
- (26) Leu, C.-M.; Reddy, G. M.; Wei, K.-H.; Shu, C.-F. *Chem. Mater.* **2003**, *15*, 2261–2265.
- (27) Sullivan, L. M.; Lukehart, C. M. *Chem. Mater.* **2005**, *17*, 2136–2141.
- (28) Chen, X.; Gonsalves, K. E. *J. Mater. Res.* **1997**, *12*, 1274–1286.
- (29) Devaraju, N. G.; Kim, E. S.; Lee, B. I. *Microelectron. Eng.* **2005**, *82*, 71–83.
- (30) Kong, Y.; Du, H.; Yang, J.; Shi, D.; Wang, Y.; Zhang, Y.; Xin, W. *Desalination* **2002**, *146*, 49–55.
- (31) Siochi, E. J.; Working, D. C.; Park, C.; Lillehei, P. T.; Rouse, J. H.; Topping, C. C.; Bhattacharyya, A. R.; Kumar, S. *Composites, Part B* **2004**, *35*, 439–446.
- (32) Deitzel, J. M.; Kleinmeyer, J.; Harris, D.; Beck Tan, N. C. *Polymer* **2001**, *42*, 261–272.

- (33) Zhang, H. B.; Jayasinghe, S. N.; Edirisinghe, M. J. *J. Electroanal. Chem.* **2006**, *64*, 355–360.
- (34) Koerner, T.; Turck, K.; Brown, L.; Oleschuk, R. D. *Anal. Chem.* **2004**, *76*, 6456–6460.
- (35) Baumgarten, P. K. *J. Colloid Interface Sci.* **1971**, *36*, 71–79.
- (36) Fong, H.; Chun, I.; Reneker, D. H. *Polymer* **1999**, *40*, 4585–4592.
- (37) Reneker, D. H.; Yarin, A. L.; Fong, H.; Koombhongse, S. *J. Appl. Phys.* **2000**, *87*, 4531–4547.
- (38) Zhang, D.; Karki, A. B.; Rutman, D.; Young, D. P.; Wang, A.; Cocke, D.; Ho, T. C.; Guo, Z. *Polymer* **2009**, *50*, 4189–4198.
- (39) Meesters, G. M. H.; Zevenhoven, C. A. P.; Brons, J. F. J.; Verheijen, P. J. T. *J. Electroanal. Chem.* **1990**, *25*, 265–275.
- (40) Grace, J. M.; Marijnissen, J. C. M. *J. Aerosol Sci.* **1994**, *25*, 1005–1019.
- (41) Reneker, D. H.; Chun, I. *Nanotechnology* **1996**, *7*, 216–223.
- (42) Li, D.; Xia, Y. *Adv. Mater.* **2004**, *16*, 1151–1170.
- (43) Beachley, V.; Wen, X. *Mater. Sci. Eng., C* **2009**, *29*, 663–668.
- (44) Tin, P. S.; Chung, T. S.; Liu, Y.; Wang, R.; Liu, S. L.; Pramoda, K. P. *J. Membr. Sci.* **2003**, *225*, 77–90.
- (45) Ding, Y.; Bikson, B. *Polymer* **2010**, *51*, 46–52.
- (46) Lu, H.; Nutt, S. *Macromolecules* **2003**, *36*, 4010–4016.
- (47) Dai, X.; Xu, J.; Guo, X.; Lu, Y.; Shen, D.; Zhao, N.; Luo, X.; Zhang, X. *Macromolecules* **2004**, *37*, 5615–5623.
- (48) Uthirakumar, P.; Nahm, K. S.; Hahn, Y. B.; Lee, Y.-S. *Eur. Polym. J.* **2004**, *40*, 2437–2444.
- (49) Guo, Z.; Zhang, D.; Wei, S.; Wang, Z.; Karki, A. B.; Li, Y.; Bernazzani, P.; Young, D. P.; Gomes, J. A.; Cocke, D. L.; Ho, T. C. *J. Nanopart. Res.* DOI: 10.1007/s11051-009-9802-z. Published Online: Nov 19, 2009.
- (50) Xie, X.-L.; Liu, Q.-X.; Li, R. K.-Y.; Zhou, X.-P.; Zhang, Q.-X.; Yu, Z.-Z.; Mai, Y.-W. *Polymer* **2004**, *45*, 6665–6673.
- (51) Shi, Y.; Peterson, S.; Sogah, D. Y. *Chem. Mater.* **2007**, *19*, 1552–1564.
- (52) Guo, Z.; Lei, K.; Li, Y.; Ng, H. W.; Prikhodko, S.; Hahn, H. T. *Compos. Sci. Technol.* **2008**, *68*, 1513–1520.
- (53) Guo, Z.; Lin, H.; Karki, A. B.; Wei, S.; Young, D. P.; Park, S.; Willis, J.; Hahn, T. H. *Compos. Sci. Technol.* **2008**, *68*, 2551–2556.
- (54) Cullity, B. D.; Graham, C. D. *Introduction to magnetic materials*, 2nd ed.; John Wiley & Sons: Hoboken, NJ, 2009; p 531.
- (55) Dimitrov, D. V.; Hadjipanayis, G. C.; Papaefthymiou, V.; Simopoulos, A. *J. Vac. Sci. Technol., A* **1997**, *15*, 1473–1477.

JP1020033